



HAL
open science

Mixed-Reference Spin-Flip Time-Dependent Density Functional Theory for Accurate X-ray Absorption Spectroscopy

Woojin Park, Marc Alías-Rodríguez, Daeheum Cho, Seunghoon Lee, Miquel Huix-Rotllant, Cheol Ho Choi

► **To cite this version:**

Woojin Park, Marc Alías-Rodríguez, Daeheum Cho, Seunghoon Lee, Miquel Huix-Rotllant, et al.. Mixed-Reference Spin-Flip Time-Dependent Density Functional Theory for Accurate X-ray Absorption Spectroscopy. *Journal of Chemical Theory and Computation*, 2022, 10.1021/acs.jctc.2c00746 . hal-03790799

HAL Id: hal-03790799

<https://hal.science/hal-03790799>

Submitted on 28 Sep 2022

HAL is a multi-disciplinary open access archive for the deposit and dissemination of scientific research documents, whether they are published or not. The documents may come from teaching and research institutions in France or abroad, or from public or private research centers.

L'archive ouverte pluridisciplinaire **HAL**, est destinée au dépôt et à la diffusion de documents scientifiques de niveau recherche, publiés ou non, émanant des établissements d'enseignement et de recherche français ou étrangers, des laboratoires publics ou privés.

Mixed-Reference Spin-Flip Time-Dependent Density Functional Theory for Accurate X-ray Absorption Spectroscopy

Woojin Park,^{†,‡} Marc Alías-Rodríguez,^{¶,‡} Daeheum Cho,[†] Seunghoon
Lee,[§] Miquel Huix-Rotllant,^{*,¶} and Cheol Ho Choi^{*,†}

[†]*Department of Chemistry, Kyungpook National University, Daegu 41566, South Korea*

[‡]*contributed equally*

[¶]*Aix-Marseille Univ, CNRS, ICR, Marseille, France*

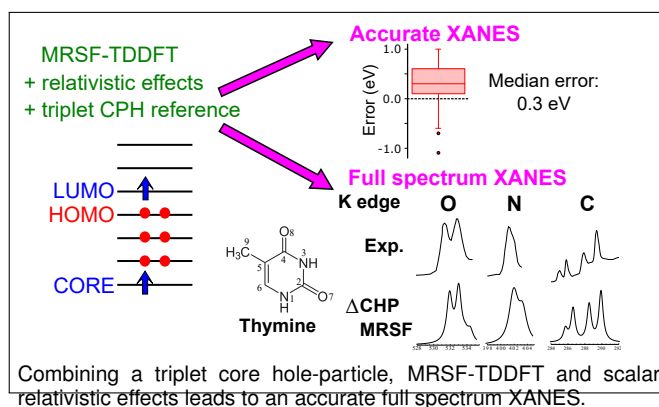
[§]*Division of Chemistry and Chemical Engineering, California Institute of Technology, Pasadena,
California 91125, USA*

E-mail: miquel.huix-rotllant@cnrs.fr; cchoi@knu.ac.kr

Abstract

It is demonstrated that the challenging *core hole-particle* (CHP) orbital relaxation for core electron spectra can be readily achieved by the mixed-reference spin-flip (MRSF)-TDDFT. With the additional scalar relativistic effects on K-edge excitation energies of 24 second- and 17 third-row molecules, the particular Δ CHP-MRSF(R) exhibited near perfect predictions with RMSE ~ 0.5 eV, featuring a median value of 0.3 and an interquartile range of 0.4. Overall, the CHP effect is 2 \sim 4 times stronger than relativistic ones, contributing more than 20 eV in the cases of sulfur and chlorine third-row atoms. Such high precision allows to explain the splitting and spectral shapes of O, N and C atom K-edges in the ground state of thymine with atom as well as orbital specific accuracy. The same protocol with a *double hole particle* relaxation also produced remarkably accurate K-edge spectra of *core to valence hole* excitation energies from the first ($n_{O8}\pi^*$) and second ($\pi\pi^*$) excited states of thymine, confirming the assignment of $1s \rightarrow n$ excitation for the experimentally observed 526.4 eV peak. Regarding both accuracy and practicality, therefore, MRSF-TDDFT provides a promising protocol for core electron spectra both of ground and excited electronic states alike.

TOC Graphic



Introduction

Recent experimental advances like the X-ray free-electron lasers (XFELs)¹ that generate intense, coherent and short light X-ray pulses have drawn significant attention to X-ray spectroscopy,² which can potentially probe chemical events with a time resolution ranging from attoseconds to few femtoseconds. As opposed to valence states, which usually probe delocalized states, core excitation energies are energetically well-separated, and the corresponding core orbitals are spatially localized on a single or a few atoms, allowing highly element-specific techniques. This is particularly useful when X-ray spectroscopy is used as a probe for ultrafast dynamic processes, leading to the time-resolved (TR) variants of X-ray absorption (TRXAS), photoelectron (TRXPS), etc. X-ray spectroscopy, especially when used as a probe, requires an accurate theoretical interpretation. Correspondingly, there have been intense activities toward accurate and computationally efficient theoretical predictions of X-ray absorption spectroscopy (XAS). Nowadays, most quantum chemistry methods can be used to extract core excitation states. Currently, the best accuracy is provided by many electron wave function methods, such as complete active space self-consistent field with multi-configurational perturbation theory,³ coupled cluster,⁴⁻⁷ restricted active space self-consistent field,⁸ or linear-response methods like the algebraic diagrammatic construction,^{9,10} linear-response complete-active space self-consistent field,¹¹ and Bethe-Salpeter equation (BSE) formalism,¹² just to mention a few. Still, their applicability is usually hindered by their computational cost.

Linear-response time-dependent density functional theory (TDDFT)¹³ has been the most popular method for valence excited state studies due to its computational simplicity and efficiency. Given a set of reference orbitals (usually obtained by Kohn-Sham DFT), TDDFT can produce a full spectrum of excited states in one shot at a reasonable level of accuracy, giving access to excited state energies and inter-state properties such as transition dipole-moment (TDM), non-adiabatic coupling (NAC), spin-orbit coupling (SOC), etc. TDDFT can also be applied to core excitations. Applying TDDFT to X-ray spectroscopy requires, in practice, to limit the single excitation space, as recovering the high-lying core-hole excited states would otherwise

require the full diagonalization of the TDDFT matrices. To restrict the excitations to the relevant core states within TDDFT,¹⁴ approximations in the excitation space are frequently applied, like the core–valence separation (CVS)¹⁵ or restricted excitation window (REW)^{14,16–18} schemes. Still, the accuracy of TDDFT to predict experimental X-ray states is very crude, with errors as large as ~ 10 eV for second period elements like C,N,O and F,¹⁹ and even larger errors for heavier elements. Alike shifts are also needed with TDDFT variants for X-ray spectroscopy, like the recently developed hole-hole Tamm–Dancoff–approximated density functional theory (hh–TDA)²⁰ and orthogonality constrained density functional theory (OCDFT).²¹ These large shifts are attributed to the lack of description of *core-hole orbital relaxation* effects in the approximate exchange-correlation functionals used in TDDFT, which cannot account for the drastic change in the Coulomb interaction of the remaining electrons when a core electron is excited. A simple remedy to orbital relaxation is not available in the context of TDDFT approach, despite some attempts on applying linear response on a set of orbitals converged for a *core-hole* (CH) excited state, which improves the description of XAS.²² Alternatively, DFT approaches like Δ SCF²³ or the transition potential DFT²⁴ methods have been proposed as a remedy, with very good accuracy.²⁵

In recent studies, the state-specific orbital optimized (OO)–DFT methods have been actively developed,²³ featuring an unprecedented precision of DFT methods in the description of X-ray spectroscopy.²⁵ OO-DFT methods converge a singlet core hole state by employing the maximum overlap method (MOM)²⁶ to maintain the specific excited state during the self-consistent field calculation, thus accounting for orbital relaxation by construction. Recent OO–DFT with the spin-free exact two-component one-electron model (SF-X2C1e) for scalar relativistic effects,²⁵ shows a promising result. However, OO-DFT requires an independent computation for each target states, which complicates the construction of the spectrum over a broad range of spectral regions. Without a good prior knowledge of each specific excited states, a large number of candidate states have to be investigated, making the process considerably more computationally demanding with inconvenient identification processes. In addition, it is typically difficult to converge the target

core-excited state.²⁶ To cope with *core-hole* relaxation issue, OO-DFT also has to resort to the orbital optimizations with either Δ SCF or restricted open-shell Kohn-Sham (ROKS).²⁷

In this regard, LR theories are still preferable for their practicality and generality, and could be advantageous for an accurate description of X-ray spectroscopy if orbital relaxation effects are included.²² In this article, we propose the use of the recently developed mixed-reference spin-flip (MRSF)-TDDFT (MRSF for brevity in some places) as an accurate and general strategy for X-ray spectroscopy.²⁸⁻³⁰ Unlike TDDFT formalism, the major challenges of conventional LR theories mentioned above can be rather easily overcome by MRSF. It needs to be first clarified that the commonly adopted CH relaxation with an ionic system by removing one electron does not represent the lowest energy X-ray absorption states. Rather, the orbital optimization with the *core hole-particle pair* (CHP) of neutral system should be performed instead, which can be readily achieved by the high-spin restricted open-shell Hartree-Fock (ROHF) reference within the context of MRSF formalism. In this way, orbital relaxation effects are built in the SCF like in OO-DFT methods, but MRSF allows the construction of the full X-ray spectrum at once on top of that reference. In addition, by virtue of orbital Hessian diagonalization with the orbitals optimized for high energy CHP configuration, various lower energy valence states can be also obtained as byproducts. If only specific particular state(s) are needed, one can also restrict the excitation operators in linear response to particular core excitation(s) by such as CVS or REW as well, simplifying XAS computations.

Conventional LR theories have to take a single reference to ensure its corresponding density idempotent property, and hence only singly excited configurations are included. MRSF-TDDFT overcomes this limitation by a spinor-like transformation in the context of spin-flip excitations, which allows to combine the reduced density matrices (RDMs) of the two $M_S=\pm 1$ triplet-ground references within the realm of LR theory. The expanded response space provides additional nondynamic electron correlation – the missing piece of conventional LR theories, balancing dynamic and nondynamic electron correlations. Especially, the one-electron (de)-excitation and spin-flip from the restricted open-shell triplet reference Kohn-Sham determinant includes

some two-electron correlations in the form of *doubly* excited configurations, which is the main ingredient to properly account for the dark $2^1A_g^-$ states of *s-trans*-butadiene and *s-trans*-hexatriene.³¹ The same MRSF-TDDFT formulation also produces the ground singlet as one of its response states, which not only eliminates the topological problem³² of CI₁₀ (the conical intersection between ground and excited states) by TDDFT but also allows to study open shell ground singlet states.³³ *Thus, MRSF-TDDFT is equipped with balanced dynamic and nondynamic electron correlations for both ground and excited states with the convenience of single reference orbital optimization.* This allows MRSF-TDDFT to overcome the major limitations of conventional TDDFT without the spin-contamination pitfalls of spin flip (SF)-TDDFT,³⁴ while faithfully reproducing the results of the much more expensive *ab initio* wave function theories.³¹ In a series of studies,^{30,32,33,35–42} it has been demonstrated that the MRSF-TDDFT approach can also yield accurate nonadiabatic coupling matrix elements (NACMEs),^{35,37} enabling reliable non-adiabatic molecular dynamics (NAMMD) simulations,⁴² a topologically correct description of conical intersections,^{32,38,41} and accurate values of singlet–triplet gaps.^{33,36}

In the current article, by combining standard techniques such as MOM for building a CHP reference and REW for computing X-ray states, we demonstrate that the MRSF-TDDFT is a practical, efficient and very accurate protocol in the computations of X-ray spectroscopy without any major methodological restrictions. The effect of scalar relativistic effects on the core excitations is also investigated for heavier elements.

Computational Details

Mixed-Reference Spin-Flip Density Functional Theory

The advantage of having two-component reference state is shown in Fig. 1, where the $M_S = +1$ and -1 triplet components as well as their corresponding response configurations are shown with the black and red arrows, respectively. The response configurations shown by the red arrows represent the configurations missing in the conventional SF-TDDFT, the account of which largely

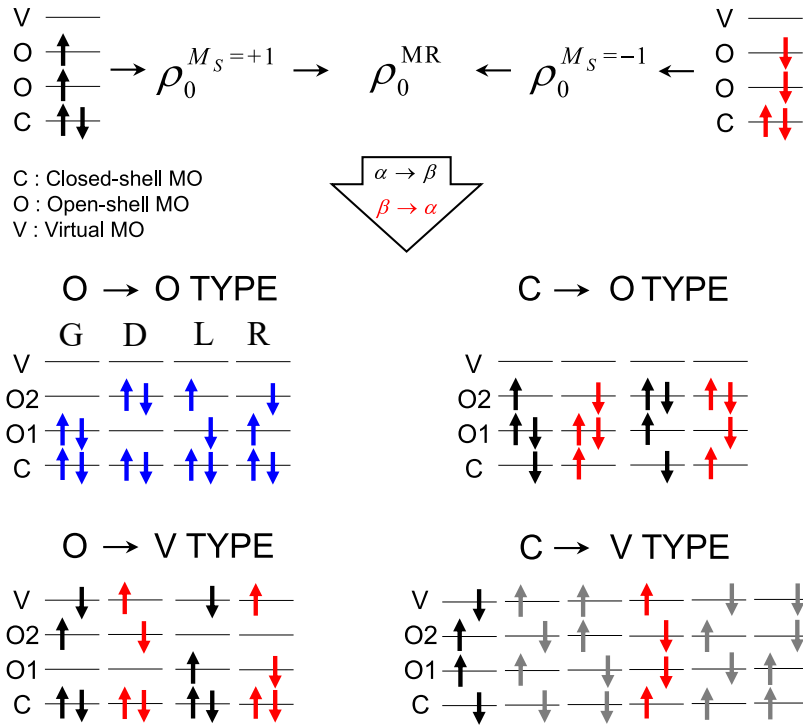


Figure 1: Upper panel shows the two references of MRSF-TDDFT denoted by black and red arrows. The zeroth-order MR-RDM which combines $M_S = +1$ and -1 RDMs is used in MRSF-TDDFT, while only the $M_S = +1$ RDM are used in SF-TDDFT. In the lower panel, the electronic configurations that can be generated by spin-flip linear responses from the MR-RDM are given by blue, black, and red arrows. The blue ones are generated from both references, which require a symmetrization procedure to eliminate the OO-type spin contamination. The black and red ones are generated from $M_S = +1$ and -1 references, respectively. By contrast, those of SF-TDDFT are only the blue and black ones. Configurations that cannot be obtained even in the MRSF-TDDFT are denoted by gray dashed arrows.

eliminates the spin contamination of the response states in MRSF-TDDFT. The $O \rightarrow O$ type configurations shown in Fig. 1 by the blue arrows originate from both $M_S = +1$ and $M_S = -1$ components of the MR state. They cover the **G**, **D**, **L** and **R** configurations defined in Fig. 1, which are important for proper description of the open-shell singlet and triplet states of diradicals. As these configurations occur in both SF and MRSF methods, it might be expected that both methods should be equally able to describe diradicals and to eliminate the spin-contamination. However, as the contributions of **L** and **R** to the SF response states depend on the particular spin-flip transitions, a mismatch between their contributions into the final response state may become a main source of the spin contamination. For example, in the SF method, the $\alpha \rightarrow \beta$ $O1 \rightarrow O1$ spin-flip transition yields the **L** configuration, whereas the $\alpha \rightarrow \beta$ $O2 \rightarrow O2$ spin-flip transition yields the **R** configuration. As the two configurations occur due to two distinct spin-flip transitions, their contributions into the final SF response state may become unequal, which may yield substantial spin-contamination. The problem of the mismatch of the contributions of the **L** and **R** configurations was solved in MRSF by externally contracting the same configurations originating from the different spin-flip orbital transitions from the two components, $M_S = +1$ and $M_S = -1$, of the MR state.²⁸

It is noteworthy that not all of the electronic configurations shown in Fig. 1 can be recovered using the MR-RDM. Thus, four out of six type IV configurations (i.e., those shown by the gray arrows in Fig. 1) remain unaccounted for. Typically, these configurations represent high-lying excited states and make insignificant contributions to the low-lying states of organic molecules.²⁸ Thus, the effect of the missing configurations on the spin contamination is expected to be small.

Core-Hole Particle Pair Relaxation by Maximum Overlap Method

Singlet, triplet and quintet response states ($M_S = 0$) are obtained by a single spin-flip excitation from $M_S = +1$ and -1 triplet-ground references, where the latter is obtained from the $M_S = +1$ reference without further calculations. The orbital optimizations of *core-hole particle pair* configuration can be accomplished by replacing the two singly occupied open ($O1$ and $O2$) orbitals

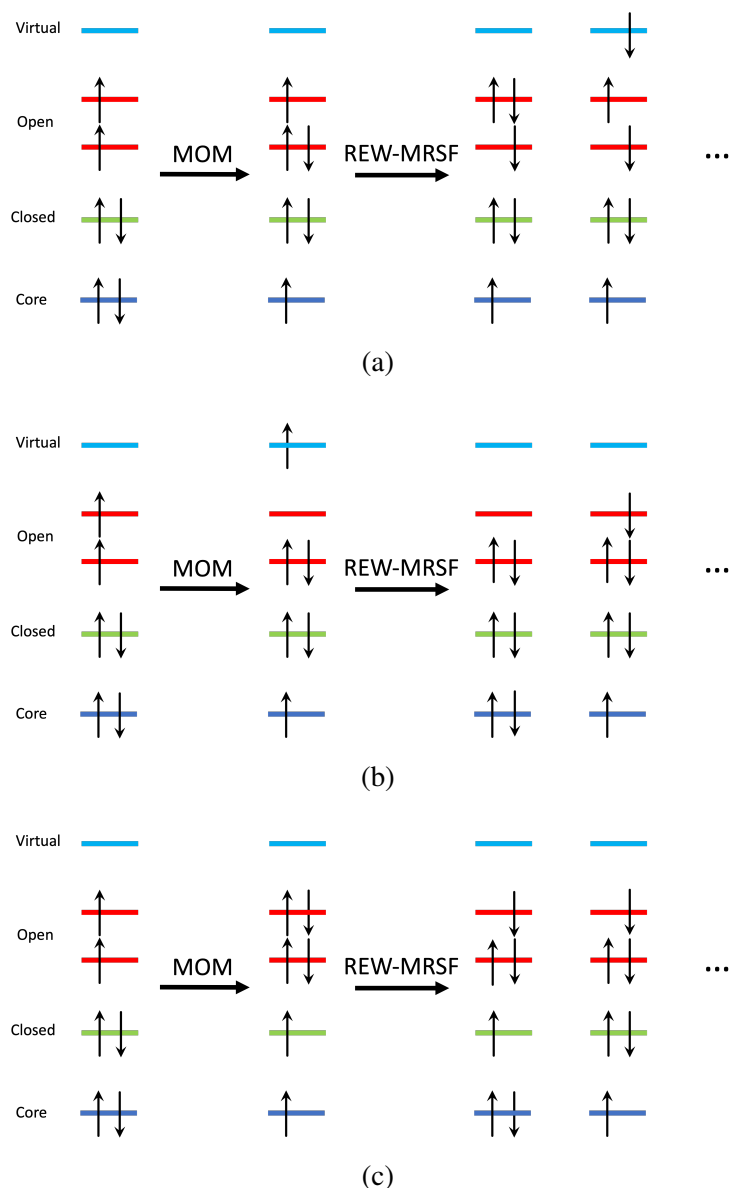


Figure 2: The *core-hole particle pair relaxation* (CHP) is accomplished by replacing the two singly occupied open (O1 and O2) orbitals of ROHF reference with other ones. While the O1 is replaced with $1s$, the O2 can be (a) the original LUMO, (b) one of virtuals or (c) one of closed orbitals. The unwanted excitation can be restricted by the restricted excitation window (REW) method.^{14,16–18} The XAS predictions with and without CHP are denoted as CHP-MRSF and MRSF respectively in the current article, all in conjunction with REW. Since the regular orbital optimizations without CHP can better represent the electron configuration before X-ray absorption, a third protocol Δ CHP-MRSF is also tested, where XAS is computed by $E(\text{CHP-MRSF}) - E(\text{RHF})$, where the $E(\text{RHF})$ can be either the singlet ground state or the singlet ground response state of MRSF-TDDFT. See Fig. S1 for the flowchart.

of ROHF reference with the particular core (the $1s$ orbital for K-edge XAS) and the virtual orbitals with the help of MOM (See Figure 2). Typically O1 and O2 are HOMO (H) and LUMO (L) with respect to RHF (HOMO: the highest occupied molecular orbital; LUMO: the lowest unoccupied molecular orbital). While the HOMO (O1) is replaced with $1s$, the O2 can be either the original LUMO (2a) or one of virtuals (2b). In the special case of Figure 2c, the O2 is replaced with one of doubly occupied closed orbitals to represent a valence *hole*. Subsequently, the mixed-reference spin-flip operations of MRSF-TDDFT generates multiple states including ground singlet and various XAS related states.

To account for both *core* as well as *valence* hole relaxations, the two singly occupied open (O1 and O2) orbitals of ROHF reference are replaced with a particular $1s$ core and a particular valence hole (either n or π hole) orbitals during SCF as presented in Table S3. This particular orbital optimization is denoted as a *double hole particle* orbital optimization as described in Figure 2c, which can be utilized for the XAS of valence excited states.

Restricted Excitation Window Scheme

To simplify the excitation space, a REW is also implemented and applied to all calculations, which restricts MRSF-TDDFT excitation space from unwanted occupied orbitals that would generate the UV-visible spectrum first. The XAS predictions with and without CHP are denoted as CHP-MRSF and MRSF respectively in the current article, all in conjunction with REW. Since the regular orbital optimizations without CHP can better represent the electron configuration before X-ray absorption, a third protocol Δ CHP-MRSF is also tested, where XAS is computed by $E(\text{CHP-MRSF}) - E(\text{RHF})$, where the $E(\text{RHF})$ can be the singlet ground state of DFT and oscillator strengths are taken from CHP-MRSF.

Scalar Relativistic Corrections

Core-hole states corresponding to $1s \rightarrow$ valence excitation can be largely affected by relativistic (R) effects due to the proximity of core electrons to the nuclei, strongly modifying the eigenvalue

spectrum, especially for atoms beyond the second period. Scalar relativistic effects have been approximately introduced to the non-relativistic (NR) Hamiltonian through the second-order Douglas-Kroll-Hess (DKH2) transformation, offering a good compromise between accuracy and computational efficiency for second and third period elements.⁴³

The MRSF-TDDFT computations were performed with a locally modified version of the GAMESS-US code as described in Refs. 28,29, which will be soon released officially. The TDDFT in conjunction with REW computations were performed with NWChem.⁴⁴ To ensure a core orbital localization,^{45,46} a core-hole correlated mixed basis set scheme was adopted, where the aug-pcX-2⁴⁷ is utilized for the atom having the core-hole, while the rest of atoms are treated by aug-pcseg-1⁴⁸ for second-row compounds and cc-pVDZ⁴⁹ for third-row compounds.⁵⁰ The former combination was utilized successfully by Head-Gordon and co-workers.^{25,51}

Experimental geometries were taken from the NIST database⁵² whenever possible, while geometries optimized at MP2/cc-pVTZ were used in their absence.⁵⁰ Economic all electron 6-31G* basis set was also utilized for comparison. To simulate TRXAS, we used NAMD trajectories from our recent work on thymine.⁴² At every 5fs of snapshots, relevant properties were computed. For all calculations, BH&HLYP⁵³ functional was employed. As was pointed out by Huix-Rotllant et al.,⁵⁴ within the widely used collinear (one-component) SF formalism, the configurations obtained by different SF transitions couple through the exact exchange only. As the current implementation of MRSF utilizes the collinear formalism, it requires a larger fraction of the exact exchange, such as in the BH&HLYP functional. Therefore, all the calculations were carried out using the BH&HLYP⁵³ hybrid exchange-correlation functional. The standard orbital rotation restriction method in GAMESS-US, which is based on MOM was adopted to obtain CHP references.

Results and Discussions

Benchmarks

The accuracy of various flavors of MRSF for X-ray spectroscopy (see Fig. 2) were systematically investigated with the help of MOM and REW on the lowest dipole allowed K-edge excitation energies of 41 small molecules and presented in Table 1, compared to the corresponding experimental data. Previous theoretical studies with OO-DFT⁵⁰ are also shown, which can be considered as reference for the accuracy of DFT-based methods for X-ray spectroscopy. All calculations of X-ray excitation energies were performed with and without scalar relativistic effects, which are designated as R and NR in the table, respectively. This allows us to comparatively estimate the contributions of scalar relativistic corrections and orbital relaxation. The latter is often attributed to the failure of TDDFT to describe X-ray core excitations accurately. The relativistic contribution is computed as the mean value of the excitation energy difference between relativistic and non-relativistic calculations in the three flavors. The orbital relaxation contribution is computed as the mean value of the state energy difference between the CHP-MRSF and MRSF computations in the R and NR forms. The Table is separated into two blocks, corresponding to the second- and third-row elements.

The statistical analysis in the form of boxplots for the data is shown in Fig. 3. As it can be observed, the best performing Δ CHP-MRSF(R) exhibited near perfect predictions of RMSE ~ 0.5 eV, featuring a median value of 0.3 and an interquartile range (IQR) of 0.4. The quality of Δ CHP-MRSF(R) is statistically similar as that of OO-DFT, with median errors below 0.5 eV and a small deviation of data. As shown by Head-Gordon and coworkers, the accuracy can be further improved by varying external parameters like the basis set and the exchange-correlation functional.²⁵ A similar behavior is expected for Δ CHP-MRSF(R) in that respect. Still, Δ CHP-MRSF(R) has the obvious advantage that the full spectrum is obtained in a single calculation (*vide infra*). Obviously, the Δ CHP-MRSF(NR) gives a larger distribution of errors, mainly due to the the 3rd row elements which clearly need a relativistic treatment for a

correct description of the core orbital energies. For the 2nd row elements on the other hand, with tiny relativistic contributions, are represented in a similar quality as that of Δ CHP-MRSF(R). The CHP-MRSF seem contradictory, since CHP-MRSF(NR) results are neatly better than CHP-MRSF(R) even for 3rd row elements, with the median value of 0.4 and IQR of 5.9. We attribute this to a *cancellation of errors*, since the error in the description of the ground-state in CHP-MRSF that red-shifts the excitation energy is partially compensated by the lack of relativistic effects which induce a blue-shift due to the core relaxation. Albeit approximately, CHP-MRSF(NR) could be a promising cheap alternative to XAS K-edge spectroscopy, that can be applied when only a qualitative estimate of the excitation energy is desired. Finally, the MRSF flavors without including orbital relaxation give similar errors to TDDFT as expected, with a median of -6 eV and an IQR between 15 and 20 eV.

Frequently in the XAS theoretical literature, the lack of orbital relaxation is attributed as the main source of error between the theoretically predicted and the experimental excitation energies. Here, we estimate the orbital relaxation contributions along with the relativistic correction to decompose the sources of error of TDDFT and alike methods. As it can be seen in Table 1, the orbital relaxation contribution is systematically larger than the relativistic contribution, which is consistent with a previous study.⁵⁰ For the second-row elements, in which the nuclei are less heavy, there is no clear tendency on the size of that orbital relaxation, with similar values for C and N K-edges, and slightly larger values for O and F K-edges. On the contrary, the atoms of the 3rd row clearly show that the increase of mass of the atom implies a larger orbital relaxation and relativistic contributions. For such cases, the orbital relaxation is 2-4 times larger than the relativistic contribution.

Table 1: Lowest dipole allowed K-edge excitation energies (in eV) for 41 small molecules.^{a)}
See Table S1 for energy difference with respect to experimental values.

	Exp.	Δ CHP-MRSF		CHP-MRSF		MRSF		Contribution		OO (SCAN/BHLLYP) ^{25,51}
		R	NR	R	NR	R	NR	Orb.	R.	
HCHO	285.6 ⁵⁵	286.5	286.4	286.1	286.0	283.5	283.4	2.4	0.1	285.8
HCN	286.4 ⁵⁶	286.7	286.6	286.4	286.3	285.0	284.9	1.1	0.1	286.4
CO	287.4 ⁵⁷	287.2	287.1	288.0	287.9	282.3	282.2	5.5	0.1	287.1
CH ₄	288.0 ⁵⁸	287.3	287.2	286.5	286.4	283.1	283.0	4.4	0.1	288.2
CH ₃ OH	288.0 ⁵⁹	289.0	288.8	288.1	288.0	286.8	286.7	1.9	0.1	288.2
HCOOH	288.1 ⁵⁹	288.6	288.5	287.9	287.8	285.3	285.2	2.6	0.1	288.0
HCOF	288.2 ⁶⁰	289.1	289.0	289.3	289.1	285.4	285.3	3.0	0.1	288.2
CO ₂	290.8 ⁶¹	291.2	291.0	291.5	291.4	290.8	290.7	0.6	0.1	290.4
CF ₂ O	290.9 ⁶⁰	291.0	290.9	290.6	290.5	287.5	287.4	3.1	0.1	290.6
HCN	399.7 ⁵⁶	399.8	399.6	397.8	397.6	394.2	394.0	5.0	0.2	399.7
NH ₃	400.8 ⁵⁸	401.2	401.0	399.7	399.5	395.8	395.6	5.3	0.2	400.5
Glycine (N)	401.2 ⁶²	401.7	401.5	399.9	399.6	400.6	400.4	0.4	0.2	401.1
Pyrrrole (N)	402.3 ⁶³	402.6	402.3	400.6	400.4	401.9	401.7	1.1	0.2	402.3
HCHO	530.8 ⁵⁵	531.0	530.6	528.1	527.7	525.0	524.6	5.3	0.4	530.9
Me ₂ CO	531.4 ⁵⁹	531.6	531.2	528.5	528.1	525.2	524.8	5.4	0.4	531.3
HCOF	532.1 ⁶⁰	532.1	531.7	529.5	529.1	525.7	525.3	5.6	0.4	532.1
CF ₂ O	532.7 ⁶⁰	533.3	532.9	530.7	530.3	526.4	526.0	6.1	0.4	533.1
H ₂ O	534.0 ⁵⁸	534.6	534.2	532.9	532.5	528.2	527.8	6.1	0.4	533.9
CH ₃ OH	534.1 ⁵⁹	534.3	534.0	532.2	531.8	528.6	528.3	5.4	0.3	534.0
CO	534.2 ⁵⁷	533.9	533.5	532.1	531.7	532.5	532.2	1.8	0.3	534.2
NNO	534.6 ⁶¹	535.2	534.8	533.2	532.8	529.4	529.1	5.4	0.4	535.1
Furan (O)	535.2 ⁶⁴	535.4	535.0	532.6	532.2	533.6	533.2	1.4	0.4	535.2
HF	687.4 ⁶⁵	687.7	687.0	687.0	686.3	680.7	680.1	6.8	0.7	687.5
HCOF	687.7 ⁶⁰	687.9	687.3	686.2	685.5	684.6	683.9	2.6	0.7	688.0
RMSE		0.5	0.4	1.6	1.9	4.3	4.6			0.2
SiH₄	1842.5 ⁶⁶	1843.4	1839.0	1851.5	1847.1	1827.0	1822.7	16.2	4.3	1843.4
SiF₄	1849.0 ⁶⁶	1849.5	1845.2	1858.8	1854.4	1831.7	1827.4	17.5	4.3	1849.4
SiCl₄	1846.0 ⁶⁶	1846.7	1842.4	1855.0	1850.6	1830.2	1826.0	16.3	4.3	1846.5
SiBr₄	1845.0 ⁶⁶	1845.8	1841.5	1853.7	1849.3	1829.4	1825.2	16.2	4.3	1845.6
PH₃	2145.8 ⁶⁷	2146.3	2140.5	2156.4	2150.5	2128.3	2122.6	18.0	5.8	2146.3
PF₃	2149.3 ⁶⁷	2149.6	2143.8	2160.4	2154.5	2131.1	2125.4	18.3	5.8	2150.0
PF₅	2155.0 ⁶⁷	2155.2	2149.4	2165.7	2159.8	2136.4	2130.7	18.5	5.8	2155.5
POF₃	2153.3 ⁶⁷	2153.6	2147.8	2164.2	2158.3	2134.8	2139.2	18.2	5.8	2153.9
H ₂ S	2472.7 ⁶⁸	2473.0	2465.3	2484.4	2476.6	2452.4	2444.9	20.4	7.7	2472.9
SO ₂	2473.2 ⁶⁸	2473.1	2465.4	2485.0	2477.1	2453.2	2445.6	19.5	7.7	2473.4
SF ₆	2486.0 ⁶⁸	2486.4	2479.0	2497.5	2490.7	2462.6	2455.1	23.5	7.2	2486.5
SF ₅ Cl	2483.5 ⁶⁹	2484.1	2476.4	2495.4	2487.6	2459.8	2452.5	23.8	7.6	2483.9
SF ₄	2477.3 ⁷⁰	2477.8	2470.1	2489.3	2481.4	2457.3	2449.7	20.2	7.7	2478.0
HCl	2823.9 ⁷¹	2823.7	2813.7	2836.9	2826.8	2800.6	2790.8	22.8	10.0	2823.7
CH ₃ Cl	2823.4 ⁷²	2823.5	2813.5	2836.1	2826.0	2800.6	2790.9	22.5	10.0	2823.6
SF ₅ Cl	2821.8 ⁶⁹	2821.4	2811.5	2833.9	2823.8	2798.1	2788.9	22.3	9.7	2821.6
Cl ₂	2821.3 ⁷¹	2820.7	2810.8	2833.2	2823.1	2799.1	2789.3	21.4	10.0	2820.9
RMSE		0.5	7.1	11.2	4.2	20.0	26.6			0.5
Median Err.		0.3	-0.4	0.5	0.4	-6.3	-6.7			0.1
IQR		0.4	5.7	12.4	5.9	15.4	20.4			0.5

^{a)} The site of the excitation is boldfaced or specified within parentheses. Experimental values (Exp.) are compared to the scalar relativistic (R) and the non-relativistic (NR) computations of different flavors of MRSF-TDDFT. The orbital (Orb.) relaxation effect is computed as the difference between average of $E^R(\text{CHP-MRSF})$, $E^{\text{NR}}(\text{CHP-MRSF})$ and $E^R(\text{MRSF})$, $E^{\text{NR}}(\text{MRSF})$ of the given state. Similarly, the relativistic (R.) relaxation effect is approximately estimated as the difference between average of $E^R(\Delta\text{CHP-MRSF})$, $E^R(\text{CHP-MRSF})$, $E^R(\text{MRSF})$ and $E^{\text{NR}}(\Delta\text{CHP-MRSF})$, $E^{\text{NR}}(\text{CHP-MRSF})$, $E^{\text{NR}}(\text{MRSF})$. Orbital-optimized density functional theory from Ref. 51 is also shown for comparison. Root mean squared error (RMSE) vs experiment is also reported. The statistical median and interquartile range (IQR) of error difference are also reported.

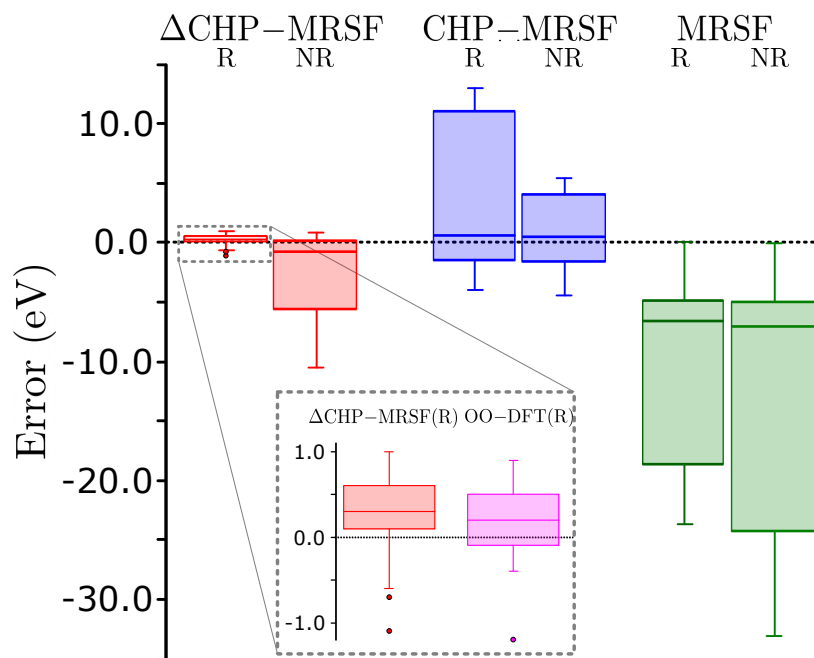


Figure 3: Boxplots for the error difference (in eV) between experiments and the three MRSF flavors for X-ray spectroscopy, both including scalar relativistic (R) and non-relativistic (NR) effects. In the offset, closeup and comparison between $\Delta\text{CHP-MRSF(R)}$ and OO-DFT(R) .

Thymine

As mentioned above, although near-edge X-ray absorption fine structure (NEXAFS) spectroscopy is one of the most powerful spectroscopic techniques to study chemical and structural effects with the ultimate sensitivity, its efficient application requires reliable complementary theoretical references. In this regard, the applicability of our best performing CHP-MRSF(NR) and Δ CHP-MRSF(R) protocols was examined by adopting the carbon, nitrogen and oxygen K-edge peaks of thymine and the results are presented in Table S2 as well as Figure 4, where the basis set effects were also investigated. Contrasting to other nucleobases, the pronounced split (531.2 and 532.8 eV) of oxygen K-edges in thymine has been either attributed to solid-state effects, i.e., the formation of a specific H-bonded configuration involving the oxygen atoms,⁷³ or methyl substitution as compared to uracil.⁷⁴

Δ CHP-MRSF(R) yielded very accurate values as compared to experiments, which allows precise peak assignments even distinguishing not only the particular atoms but also the two nearly degenerated π^* LUMO (L) and LUMO+1 (L+1) orbitals. It is noted that the oscillator strengths for Δ CHP-MRSF(R) are taken from CHP-MRSF(R) results due to nature of subtractions. For example, the two experimental peaks of 531.2 and 532.8 eV are readily assigned to O8 \rightarrow L and O7 \rightarrow L+1 transitions, respectively, since our best predicted values are 531.9 and 533.0 eV, respectively. Other possible assignments of O7 \rightarrow L and O8 \rightarrow L+1 transitions are unlikely due to their much lower oscillator strengths (See Table S2). An excellent agreement between simulated and experimental spectra of both solid film⁷³ and gas phase⁷⁵ in Figure 4a, further supports this assignment. Our prediction of gas phase system safely eliminates the solid-state effect argument. Therefore, the splitting can be attributed to the electron donating methyl substitution, which makes the 1s orbital of O8 slightly less stable than that of O7. Excellent agreements of nitrogen and carbon K-edge spectra are also seen in Figure 4b and c, respectively. Thus, we demonstrated that our protocols are capable of providing reliable reference data for experimental assignments. In general, our assignments are consistent with previous studies.⁷⁵⁻⁷⁸ Although the calculations with economic 6-31G* basis set are not as accurate as those with bigger basis sets in terms of absolute values, the

introduction of uniform shift value of 2.48 eV produces an excellent quantitative agreements for all O, N and C edges as shown in Figure 4. It is also practically important to note that our economic protocol of CHP-MRSF(NR) with a light 6-31G* basis set in combination with a proper simple shift is accurate enough in terms of relative peak orders and oscillator strengths, which can be useful in the computationally intensive calculations of time-resolved XAS simulations. Contrasting to these, the results by TDDFT exhibit a large absolute error requiring an uniform shift of 14.3 eV. However, after the correction, the relative peak positions and intensities are consistent with ours.

In the recent time-resolved experiments,² the NEXAFS spectra 2 ps after ultraviolet (UV) excitation exhibits a unique peak at 526.4 eV, which was interpreted by the core excitation channel to n hole of $n\pi^*$ valence state² on the basis of NEXAFS spectra simulations by coupled-cluster (CC) theory.

According to the recent NAMD simulations,⁴² the majority of excited populations 2ps after UV excitation reside on near $S_{1,min}$ ($n_{O8}\pi^*$) by way of the initial FC ($S_2 \pi\pi^*$ excitation) and the conical intersection between S_2 and S_1 (CI_{21}). The corresponding $1s$ core excitation spectra either of $\pi\pi^*$ (π hole) and $n\pi^*$ (n hole) states of the three particular structures were simulated by Δ CHP-MRSF(R) and the results are presented in Figure 5 and Table S3. To account for both *core* as well as *valence* hole relaxations, the two singly occupied open (O1 and O2) orbitals of ROHF reference are replaced with a particular $1s$ core and a particular valence hole (either n or π hole) orbitals during SCF as presented in Table S3 as described in Computational Details.

Remarkably, a near perfect $1s(O_8) \rightarrow n(O_8)$ core to valence n hole excitation value of 526.8 eV at $S_{1,min}$ is predicted without any empirical shift, supporting the experimental assignment.² An equally strong second band of 532.8 eV ($1s(O_7) \rightarrow \pi^*+1$) is also seen, which is gradually red-shifted to 532.6 (CI_{21} at S_1) \rightarrow 532.5 (CI_{21} at S_2) \rightarrow 532.3 eV (FC at S_2). This peak exactly overlaps with the experimental 532.8 eV peak of ground state. Although the ground state bleaching (GSB) near 531.4 eV was interpreted as a direct signature of the ground-state depopulation and assumed largely independent of any following excited-state dynamics,² it is not clear that why it only appears in the first peak of the doublet. Perhaps, our peak of 532.8 eV at S_1 eliminates the

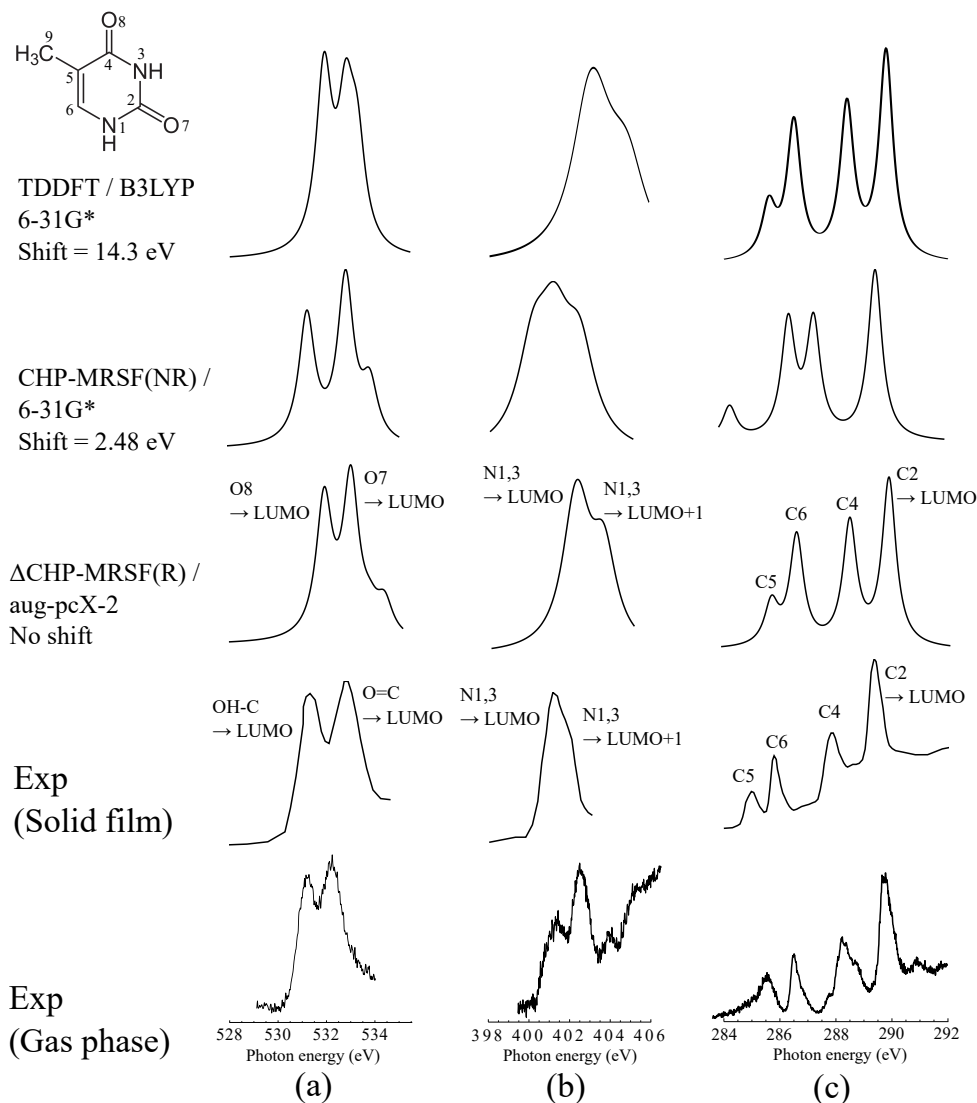


Figure 4: The (a) O, (b) N, and (c) C K-edge XAS of a ground state thymine by TDDFT/B3LYP with 6-31G* (first row), CHP-MRSF(NR) with 6-31G* (second row) and Δ CHP-MRSF(R) with aug-pcX-2/aug-pcseg-1 (third row) in comparison with experiments taken from Ref. 73 (fourth row: solid film) and Ref. 75 (fifth row: gas phase). Oscillator strengths for Δ CHP-MRSF(R) are taken from CHP-MRSF(R) results. IUPAC atom numbering of thymine is given.

GSB of the second peak. A weak and red-shifted 525.2 eV peak ($1s(O_8) \rightarrow \pi$) appears at FC geometry at S_2 , which is gradually blue-shifted to 526.4 eV at conical intersection (CI_{21} at S_2). A relatively weak but distinct secondary 527.9 eV peak ($1s(O_7) \rightarrow \pi$) also appears, which may explain a very weak experimental band near 527 ~ 529 eV. However, the secondary peak at the same CI_{21} disappears in S_1 state due to the different valence holes (n vs. π) and only produces

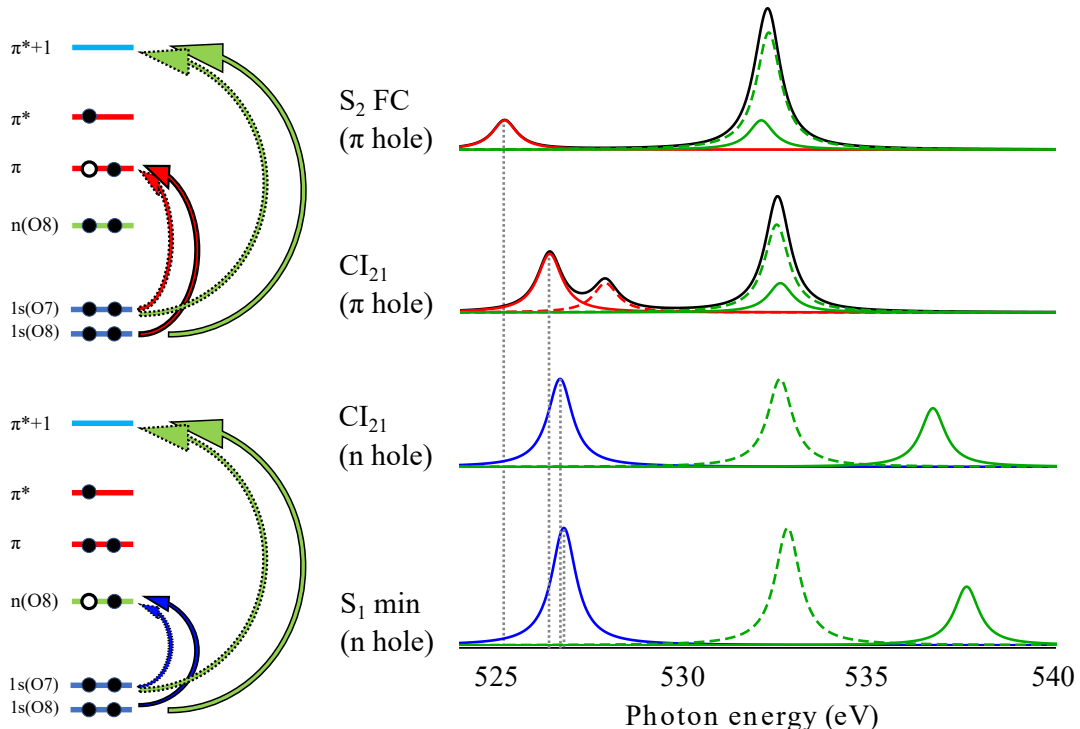
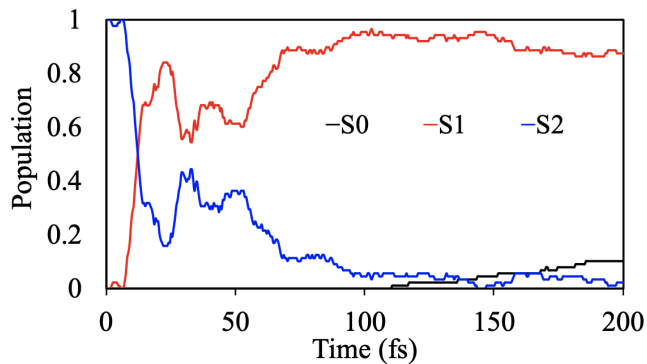


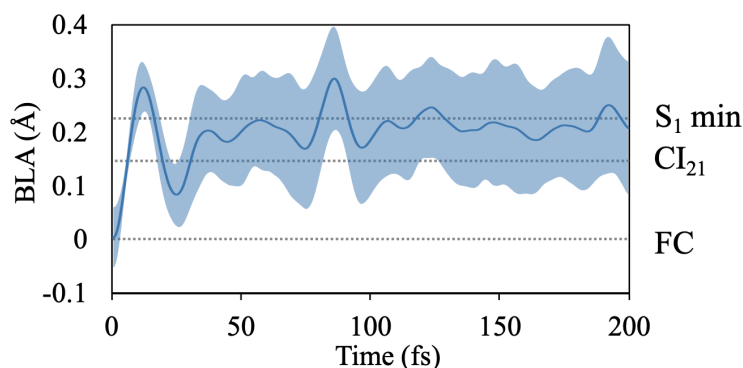
Figure 5: The simulated *core to valence hole* spectra without an empirical shift and corresponding orbital transition diagrams of valence excited states of thymine by Δ CHP-MRSF(R)/BH&HLYP with aug-pcX-2/aug-pcseg-1, where the π and n holes are represented by blank circles. Oscillator strengths for Δ CHP-MRSF(R) are taken from CHP-MRSF(R) results. The core to π , n and $\pi^* + 1$ holes are represented by red, blue and green colors. The solid and dotted lines represent the excitations from $1s(O_8)$ and $1s(O_7)$ core, respectively (See Fig. 4 for atom numbering). Here, we introduces a *double hole particle* relaxation, which relaxes a core and a valence hole at the same time. For example, the final configuration of $1s^1 n^2 \pi^{*1}$, which is $1s \rightarrow n$ core excitation of $n_{O_8} \pi^*$ state can be accomplished by the $\pi^* \rightarrow n$ response excitation from the reference *double hole particle* CHP configuration of $1s^1 n^1 \pi^{*2}$.

the 526.7 eV peak ($1s(O_8) \rightarrow n(O_8)$). In the higher energy region, a peak near 536.7 ~ 537.6 eV ($1s(O_8) \rightarrow \pi^* + 1$) either from CI_{21} (S_1) or $S_{1,min}$ overlaps with the ionization at 537 eV and additional weak resonant transitions.⁷⁵

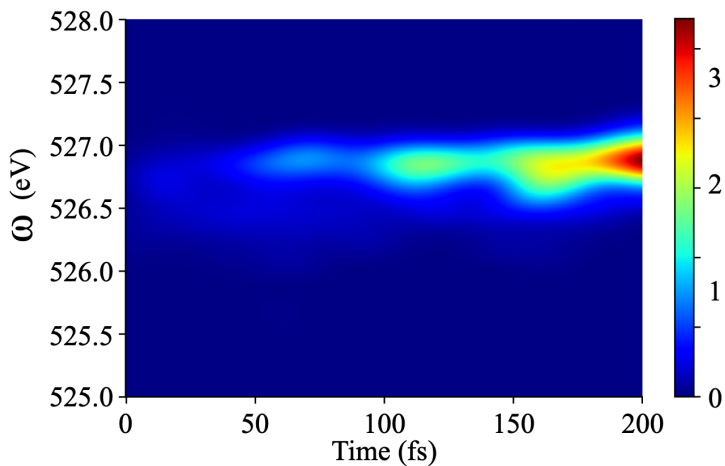
Using the trajectories obtained in our previous study,⁴² theoretical TRXAS up to 200 fs was simulated by only adopting $1s(O_8)$ *core to valence hole* ($1s(O_8) \rightarrow n(O_8)$ and $1s(O_8) \rightarrow \pi$) excitations and the results are presented in Figure 6(c) along with the population and BLA (bond length alternation) changes. According to the population change in Figure 6(a), the $\pi\pi^*$ (S_2)



(a)



(b)



(c)

(a)

Figure 6: (a) The electronic state population changes of S_2 , S_1 and S_0 from the thymine NAMD trajectories. (b) The averaged BLA ($= \frac{1}{2}(\Delta R_{C_4=O_8} + \Delta R_{C_5=C_6}) - \Delta R_{C_4-C_5}$) and corresponding standard deviation during NAMD runs, where ΔR 's are displacements with respect to the S_0 equilibrium geometry. (c) The O_8 oxygen K-edge TRXAS of thymine up to 200 fs by Δ CHP-MRSF(R) with aug-pcX-2/aug-pcseg-1. See Fig. 4 for atom numbering. Oscillator strengths for Δ CHP-MRSF(R) are taken from Δ CHP-MRSF(R) results.

$\rightarrow n_{O8\pi^*}(S_1)$ population transfer is nearly completed within 100 fs. Therefore, the TRXAS upto 200 fs represents the sequence of 525.2 (FC at S_2) \rightarrow 526.4 (CI_{21} at S_2) \rightarrow 526.7 (CI_{21} at S_1) \rightarrow 526.8 eV ($S_{1,min}$) peak changes. A gradual intensity increase of 526 \sim 527 eV range is seen as a function of time in the theoretical TRXAS, which is consistent with experiment.² The intensities before 100fs are coming both from S_2 and S_1 , while they are mostly composed of S_1 excitation afterwards. Since intensities from S_2 are generally weaker, the weak intensity before 100fs in TRXAS is expected. In fact, the initial peak at 525.2 eV (FC at S_2) is nearly invisible. However, it is interesting to note that the complete population transfer to S_1 at 100 fs does not immediately enhance the intensities in Figure 6(c). The initial highly correlated BLA modes across trajectories within \sim 50 fs would not produce sufficient intensities. Rather, subsequently decoherent geometric relaxation (vibrational) as represented by the major BLA mode in Figure 6(b) is needed to exhibit its maximum XAS intensity at 200 fs. Therefore the TRXAS intensity change in the short time region (\sim 200fs) represents a strong vibronic coupling of non-adiabatic transition and vibrational relaxation.

Conclusions

With the help of MOM, REW and scalar relativistic effects, theoretical predictions of X-ray absorption spectroscopy (XAS) by recently developed MRSF-TDDFT have been investigated. We demonstrated that the preferred orbital optimization with the *core hole-particle pair* (CHP) of a neutral system rather than incomplete *core-hole* (CH) relaxation with an ionic system, can be readily achieved by the high-spin restricted open-shell Hartree-Fock (ROHF) reference within the context of MRSF-TDDFT formalism.

According to our systematic investigation of the lowest dipole allowed K-edge excitation energies of 41 small molecules, the Δ CHP-MRSF protocol with CHP orbital relaxation in combination with relativistic corrections exhibited near perfect predictions with RMSE \sim 0.5 eV. It makes unnecessary the problematic empirical energy shift of several tens of eVs of X-ray

excitation energies obtained with TDDFT. As compared to OO-DFT, Δ CHP-MRSF(R) has the obvious advantage that the full spectrum is obtained in a single calculation (*vide infra*). Overall, the CHP effect is 2 ~ 4 times stronger than relativistic ones, contributing more than 20 eV in the cases of sulfur and chlorine third-row atoms. For the CHP-MRSF flavor, the NR version is neatly better than when scalar relativistic effects are included, which can be attributed to a *cancellation of errors*. Thus, it can be a promising economic protocol, which can be applied when only a qualitative estimate of the excitation energy is desired.

In the applications on the thymine at its ground state, it was demonstrated that remarkably accurate values were predicted by Δ CHP-MRSF(R), allowing specific atom as well as specific π^* orbital assignments, safely eliminating the solid-state effect argument for the peculiar oxygen K-edge splitting. In order to account for the orbital relaxation effects on the core hole as well as valence hole of electronically excited states, a *double hole particle* approach is introduced, where an orbital optimization with the two holes are performed. This approach produced a remarkably accurate prediction of the experimentally found red-shifted 526.4 eV ($1s \rightarrow n$ core excitation of $n\pi^*$ state). Thus, we demonstrated that our protocols are capable of providing absolute reference data for experimental assignments.

Acknowledgement

This work was supported by the Samsung Science and Technology Foundations (SSTF-BA1701-12) for the fundamental theory developments and the NRF funded by the Ministry of Science and ICT (2020R1A2C2008246 and 2020R1A5A1019141). This work was also supported by the Korea Polar Research Institute(KOPRI, PE22120) funded by the Ministry of Oceans and Fisheries. MAS and MHR acknowledge financial support by the “Agence Nationale pour la Recherche” through the project MULTICROSS (ANR-19-CE29-0018-01). Centre de Calcul Intensif d’Aix-Marseille is acknowledged for granting access to its high performance computing resources. We thank the financing through the program PHC STAR 2019 granted by

the “ministère de l’Europe et des Affaires étrangères” (MEAE), the “ministère de l’Enseignement supérieur, de la Recherche et de l’Innovation” (MESRI) and the National Research Foundation of Korea (NRF).

Supporting Information

A separate supporting information file is provided.

References

- (1) Pellegrini, C. The development of XFELs. *Nat. Rev. Phys.* **2020**, *2*, 330–331.
- (2) Wolf, T.; Myhre, R. H.; Cryan, J.; Coriani, S.; Squibb, R.; Battistoni, A.; Berrah, N.; Bostedt, C.; Bucksbaum, P.; Coslovich, G. et al. Probing ultrafast $\pi\pi^*/n\pi^*$ internal conversion in organic chromophores via K-edge resonant absorption. *Nat. Commun.* **2017**, *8*, 1–7.
- (3) Couto, R. C.; Cruz, V. V.; Ertan, E.; Eckert, S.; Fondell, M.; Dantz, M.; Kennedy, B.; Schmitt, T.; Pietzsch, A.; Guimarães, F. F. et al. Selective gating to vibrational modes through resonant X-ray scattering. *Nat. Commun.* **2017**, *8*, 1–7.
- (4) Coriani, S.; Koch, H. Communication: X-ray absorption spectra and core-ionization potentials within a core-valence separated coupled cluster framework. *Chem. Phys.* **2015**, *143*, 181103.
- (5) Peng, B.; Lestrangle, P. J.; Goings, J. J.; Caricato, M.; Li, X. Energy-specific equation-of-motion coupled-cluster methods for high-energy excited states: Application to K-edge X-ray absorption spectroscopy. *J. Chem. Theory Comput.* **2015**, *11*, 4146–4153.
- (6) Faber, R.; Coriani, S. Resonant inelastic X-ray scattering and nonresonant X-ray emission spectra from coupled-cluster (damped) response theory. *J. Chem. Theory Comput.* **2019**, *15*, 520–528.
- (7) Vidal, M. L.; Feng, X.; Epifanovsky, E.; Krylov, A. I.; Coriani, S. New and efficient equation-of-motion coupled-cluster framework for core-excited and core-ionized states. *J. Chem. Theory Comput.* **2019**, *15*, 3117–3133.
- (8) Montorsi, F.; Segatta, F.; Nenov, A.; Mukamel, S.; Garavelli, M. Soft X-ray Spectroscopy Simulations with Multiconfigurational Wave Function Theory: Spectrum Completeness,

- Sub-eV Accuracy, and Quantitative Reproduction of Line Shapes. *J. Chem. Theory Comput.* **2022**, *18*, 1003–1016.
- (9) Wenzel, J.; Wormit, M.; Dreuw, A. Calculating core-level excitations and X-ray absorption spectra of medium-sized closed-shell molecules with the algebraic-diagrammatic construction scheme for the polarization propagator. *J. Comput. Chem.* **2014**, *35*, 1900–1915.
- (10) Fransson, T.; Dreuw, A. Simulating X-ray emission spectroscopy with algebraic diagrammatic construction schemes for the polarization propagator. *J. Chem. Theory Comput.* **2018**, *15*, 546–556.
- (11) Helmich-Paris, B. Simulating X-ray absorption spectra with complete active space self-consistent field linear response methods. *Int. J. Quantum Chem.* **2021**, *121*, e26559.
- (12) Yao, Y.; Golze, D.; Rinke, P.; Blum, V.; Kanai, Y. All-Electron BSE@ GW Method for K-Edge Core Electron Excitation Energies. *J. Chem. Theory Comput.* **2022**, *18*, 1569–1583.
- (13) Casida, M. E.; Huix-Rotllant, M. Progress in time-dependent density-functional theory. *Annu. Rev. Phys. Chem.* **2012**, *63*, 287–323.
- (14) Stener, M.; Fronzoni, G.; de Simone, M. Time dependent density functional theory of core electrons excitations. *Chem. Phys. Lett.* **2003**, *373*, 115–123.
- (15) Cederbaum, L. S.; Domcke, W.; Schirmer, J. Many-body theory of core holes. *Phys. Rev. A* **1980**, *22*, 206.
- (16) Besley, N. A.; Noble, A. Time-Dependent Density Functional Theory Study of the X-ray Absorption Spectroscopy of Acetylene, Ethylene, and Benzene on Si(100). *J. Phys. Chem. C* **2007**, *111*, 3333–3340.
- (17) DeBeer George, S.; Petrenko, T.; Neese, F. Prediction of Iron K-Edge Absorption Spectra Using Time-Dependent Density Functional Theory. *J. Phys. Chem. A* **2008**, *112*, 12936–12943.

- (18) Zhang, Y.; Biggs, J. D.; Healion, D.; Govind, N.; Mukamel, S. Core and valence excitations in resonant X-ray spectroscopy using restricted excitation window time-dependent density functional theory. *Chem. Phys.* **2012**, *137*, 194306.
- (19) Besley, N. A.; Asmuruf, F. A. Time-dependent density functional theory calculations of the spectroscopy of core electrons. *Phys. Chem. Chem. Phys.* **2010**, *12*, 12024–12039.
- (20) Hohenstein, E. G.; Yu, J. K.; Bannwarth, C.; List, N. H.; Paul, A. C.; Folkestad, S. D.; Koch, H.; Martinez, T. J. Predictions of Pre-edge Features in Time-Resolved Near-Edge X-ray Absorption Fine Structure Spectroscopy from Hole–Hole Tamm–Dancoff-Approximated Density Functional Theory. *J. Chem. Theory Comput.* **2021**, *17*, 7120–7133.
- (21) Verma, P.; Derricotte, W. D.; Evangelista, F. A. Predicting near edge X-ray absorption spectra with the spin-free exact-two-component Hamiltonian and orthogonality constrained density functional theory. *J. Chem. Theory Comput.* **2016**, *12*, 144–156.
- (22) Attar, A. R.; Bhattacharjee, A.; Pemmaraju, C. D.; Schnorr, K.; Closser, K. D.; Prendergast, D.; Leone, S. R. Femtosecond x-ray spectroscopy of an electrocyclic ring-opening reaction. *Science* **2017**, *356*, 54–59.
- (23) Hait, D.; Head-Gordon, M. Orbital optimized density functional theory for electronic excited states. *J. Phys. Chem. Lett.* **2021**, *12*, 4517–4529.
- (24) Triguero, L.; Pettersson, L. G. M.; Ågren, H. Calculations of near-edge x-ray-absorption spectra of gas-phase and chemisorbed molecules by means of density-functional and transition-potential theory. *Phys. Rev. B* **1998**, *58*, 8097–8110.
- (25) Cunha, L. A.; Hait, D.; Kang, R.; Mao, Y.; Head-Gordon, M. Relativistic Orbital-Optimized Density Functional Theory for Accurate Core-Level Spectroscopy. *J. Phys. Chem. Lett.* **2022**, *13*, 3438–3449.

- (26) Gilbert, A. T.; Besley, N. A.; Gill, P. M. Self-consistent field calculations of excited states using the maximum overlap method (MOM). *J. Phys. Chem. A* **2008**, *112*, 13164–13171.
- (27) Kowalczyk, T.; Tsuchimochi, T.; Chen, P.-T.; Top, L.; Van Voorhis, T. Excitation energies and Stokes shifts from a restricted open-shell Kohn-Sham approach. *Chem. Phys.* **2013**, *138*, 164101.
- (28) Lee, S.; Filatov, M.; Lee, S.; Choi, C. H. Eliminating spin-contamination of spin-flip time dependent density functional theory within linear response formalism by the use of zeroth-order mixed-reference (MR) reduced density matrix. *Chem. Phys.* **2018**, *149*, 104101.
- (29) Lee, S.; Kim, E. E.; Nakata, H.; Lee, S.; Choi, C. H. Efficient implementations of analytic energy gradient for mixed-reference spin-flip time-dependent density functional theory (MRSF-TDDFT). *J. Chem. Phys.* **2019**, *150*, 184111.
- (30) Lee, S.; Park, W.; Nakata, H.; Filatov, M.; Choi, C. H. Recent advances in ensemble density functional theory and linear response theory for strong correlation. *Bull. Korean Chem. Soc.* **2022**, *43*, 17–34.
- (31) Park, W.; Shen, J.; Lee, S.; Piecuch, P.; Filatov, M.; Choi, C. H. Internal Conversion between Bright (11Bu+) and Dark (21Ag-) States in s-trans-Butadiene and s-trans-Hexatriene. *J. Phys. Chem. Lett.* **2021**, *12*, 9720–9729, PMID: 34590847.
- (32) Lee, S.; Shostak, S.; Filatov, M.; Choi, C. H. Conical Intersections in Organic Molecules: Benchmarking Mixed-Reference Spin-Flip Time-Dependent DFT (MRSF-TD-DFT) vs Spin-Flip TD-DFT. *J. Phys. Chem. A* **2019**, *123*, 6455–6462.
- (33) Horbatenko, Y.; Sadiq, S.; Lee, S.; Filatov, M.; Choi, C. H. Mixed-Reference Spin-Flip Time-Dependent Density Functional Theory (MRSF-TDDFT) as a Simple yet Accurate Method for Diradicals and Diradicaloids. *J. Chem. Theory Comput.* **2021**, *17*, 848–859.

- (34) Shao, Y.; Head-Gordon, M.; Krylov, A. I. The spin–flip approach within time-dependent density functional theory: Theory and applications to diradicals. *Chem. Phys.* **2003**, *118*, 4807–4818.
- (35) Lee, S.; Kim, E.; Lee, S.; Choi, C. H. Fast Overlap Evaluations for Nonadiabatic Molecular Dynamics Simulations: Applications to SF-TDDFT and TDDFT. *J. Chem. Theory Comput.* **2019**, *15*, 882.
- (36) Horbatenko, Y.; Lee, S.; Filatov, M.; Choi, C. H. Performance Analysis and Optimization of Mixed-Reference Spin-Flip Time-Dependent Density Functional Theory (MRSF-TDDFT) for Vertical Excitation Energies and Singlet–Triplet Energy Gaps. *J. Phys. Chem. A* **2019**, *123*, 7991.
- (37) Lee, S.; Horbatenko, Y.; Filatov, M.; Choi, C. H. Fast and Accurate Computation of Nonadiabatic Coupling Matrix Elements Using the Truncated Leibniz Formula and Mixed-Reference Spin-Flip Time-Dependent Density Functional Theory. *J. Phys. Chem. Lett.* **2021**, *12*, 4722–4728.
- (38) Baek, Y. S.; Lee, S.; Filatov, M.; Choi, C. H. Optimization of Three State Conical Intersections by Adaptive Penalty Function Algorithm in Connection with the Mixed-Reference Spin-Flip Time-Dependent Density Functional Theory Method (MRSF-TDDFT). *J. Phys. Chem. A* **2021**, *125*, 1994–2006.
- (39) Pomogaev, V.; Lee, S.; Shaik, S.; Filatov, M.; Choi, C. H. Exploring Dyson’s Orbitals and Their Electron Binding Energies for Conceptualizing Excited States from Response Methodology. *J. Phys. Chem. Lett.* **2021**, *12*, 9963–9972.
- (40) Horbatenko, Y.; Lee, S.; Filatov, M.; Choi, C. H. How Beneficial Is the Explicit Account of Doubly-Excited Configurations in Linear Response Theory? *J. Chem. Theory Comput.* **2021**, *17*, 975–984.

- (41) Kim, H.; Park, W.; Kim, Y.; Filatov, M.; Choi, C. H.; Lee, D. Relief of excited-state antiaromaticity enables the smallest red emitter. *Nat. Commun.* **2021**, *12*, 1–9.
- (42) Park, W.; Lee, S.; Huix-Rotllant, M.; Filatov, M.; Choi, C. H. Impact of the Dynamic Electron Correlation on the Unusually Long Excited-State Lifetime of Thymine. *J. Phys. Chem. Lett.* **2021**, *12*, 4339–4346.
- (43) Nakajima, T.; Hirao, K. The Douglas–Kroll–Hess Approach. *Chem. Rev.* **2012**, *112*, 385–402.
- (44) Apra, E.; Bylaska, E. J.; De Jong, W. A.; Govind, N.; Kowalski, K.; Straatsma, T. P.; Valiev, M.; van Dam, H. J.; Alexeev, Y.; Anchell, J. et al. NWChem: Past, present, and future. *J. Chem. Phys.* **2020**, *152*, 184102.
- (45) Perdew, J. P.; Parr, R. G.; Levy, M.; Balduz Jr, J. L. Density-functional theory for fractional particle number: derivative discontinuities of the energy. *Phys. Rev. Lett.* **1982**, *49*, 1691.
- (46) Hait, D.; Head-Gordon, M. Delocalization errors in density functional theory are essentially quadratic in fractional occupation number. *J. Phys. Chem. Lett.* **2018**, *9*, 6280–6288.
- (47) Ambroise, M. A.; Jensen, F. Probing basis set requirements for calculating core ionization and core excitation spectroscopy by the Δ self-consistent-field approach. *J. Chem. Theory Comput.* **2018**, *15*, 325–337.
- (48) Jensen, F. Unifying general and segmented contracted basis sets. Segmented polarization consistent basis sets. *J. Chem. Theory Comput.* **2014**, *10*, 1074–1085.
- (49) Dunning, T. H. Gaussian basis sets for use in correlated molecular calculations. I. The atoms boron through neon and hydrogen. *Chem. Phys.* **1989**, *90*, 1007–1023.
- (50) Hait, D.; Head-Gordon, M. Highly accurate prediction of core spectra of molecules at density functional theory cost: Attaining sub-electronvolt error from a restricted open-shell Kohn–Sham approach. *J. Phys. Chem. Lett.* **2020**, *11*, 775–786.

- (51) Hait, D.; Oosterbaan, K. J.; Carter-Fenk, K.; Head-Gordon, M. Computing x-ray absorption spectra from linear-response particles atop optimized holes. *J. Chem. Phys.* **2022**, *156*, 201104.
- (52) Computational Chemistry Comparison and Benchmark Database, NIST Standard Reference Database 101. 2002; <http://cccbdb.nist.gov>, Release 22, May 2022.
- (53) Becke, A. D. A new mixing of Hartree–Fock and local density-functional theories. *J. Chem. Phys.* **1993**, *98*, 1372–1377.
- (54) Huix-Rotllant, M.; Natarajan, B.; Ipatov, A.; Wawire, C. M.; Deutsch, T.; Casida, M. E. Assessment of noncollinear spin-flip Tamm–Dancoff approximation time-dependent density-functional theory for the photochemical ring-opening of oxirane. *Phys. Chem. Chem. Phys.* **2010**, *12*, 12811–12825.
- (55) Hitchcock, A.; Brion, C. Carbon K-shell excitation of C₂H₂, C₂H₄, C₂H₆ and C₆H₆ by 2.5 keV electron impact. *J. Electron Spectrosc. Relat. Phenom.* **1977**, *10*, 317–330.
- (56) Hitchcock, A.; Brion, C. Inner shell electron energy loss studies of HCN and C₂N₂. *Chem. Phys.* **1979**, *37*, 319–331.
- (57) Domke, M.; Xue, C.; Puschmann, A.; Mandel, T.; Hudson, E.; Shirley, D.; Kaindl, G. Carbon and oxygen K-edge photoionization of the CO molecule. *Chem. Phys. Lett.* **1990**, *173*, 122–128.
- (58) Schirmer, J.; Trofimov, A.; Randall, K.; Feldhaus, J.; Bradshaw, A.; Ma, Y.; Chen, C.; Sette, F. K-shell excitation of the water, ammonia, and methane molecules using high-resolution photoabsorption spectroscopy. *Phys. Rev. A* **1993**, *47*, 1136.
- (59) Prince, K. C.; Richter, R.; de Simone, M.; Alagia, M.; Coreno, M. Near edge X-ray absorption spectra of some small polyatomic molecules. *J. Phys. Chem. A* **2003**, *107*, 1955–1963.

- (60) Robin, M.; Ishii, I.; McLaren, R.; Hitchcock, A. Fluorination effects on the inner-shell spectra of unsaturated molecules. *J. Electron Spectrosc. Relat. Phenom.* **1988**, *47*, 53–92.
- (61) Prince, K.; Avaldi, L.; Coreno, M.; Camilloni, R.; De Simone, M. Vibrational structure of core to Rydberg state excitations of carbon dioxide and dinitrogen oxide. *J. Phys. B: At. Mol. Opt. Phys* **1999**, *32*, 2551.
- (62) Plekan, O.; Feyer, V.; Richter, R.; Coreno, M.; De Simone, M.; Prince, K.; Carravetta, V. An X-ray absorption study of glycine, methionine and proline. *J. Electron Spectrosc. Relat. Phenom.* **2007**, *155*, 47–53.
- (63) Pavlychev, A.; Hallmeier, K.; Hennig, C.; Hennig, L.; Szargan, R. Nitrogen K-shell excitations in complex molecules and polypyrrole. *Chem. Phys.* **1995**, *201*, 547–555.
- (64) Duflot, D.; Flament, J.-P.; Giuliani, A.; Heinesch, J.; Hubin-Franskin, M.-J. Core shell excitation of furan at the O 1s and C 1s edges: An experimental and ab initio study. *Chem. Phys.* **2003**, *119*, 8946–8955.
- (65) Hitchcock, A.; Brion, C. K-shell excitation of HF and F₂ studied by electron energy-loss spectroscopy. *J. Phys. B: At. Mol. Phys.* **1981**, *14*, 4399.
- (66) Bodeur, S.; Millié, P.; Nenner, I. Single- and multiple-electron effects in the Si 1s photoabsorption spectra of SiX₄ (X=H,D,F,Cl,Br,CH₃,C₂H₅,OCH₃,OC₂H₅) molecules: Experiment and theory. *Phys. Rev. A* **1990**, *41*, 252–263.
- (67) Cavell, R. G.; Jürgensen, A. Chemical shifts in P-1s photoabsorption spectra of gaseous phosphorus compounds. *J. Electron Spectrosc. Relat. Phenom.* **1999**, *101-103*, 125–129.
- (68) Reynaud, C.; Gaveau, M.-A.; Bisson, K.; Millié, P.; Nenner, I.; Bodeur, S.; Archirel, P.; Lévy, B. Double-core ionization and excitation above the sulphur K-edge in , and. *J. Phys. B: At. Mol. Opt. Phys* **1996**, *29*, 5403–5419.

- (69) Reynaud, C.; Bodeur, S.; Maréchal, J.; Bazin, D.; Millié, P.; Nenner, I.; Rockland, U.; Baumgärtel, H. Electronic properties of the SF₅Cl molecule: a comparison with SF₆. I. Photoabsorption spectra near the sulphur K and chlorine K edges. *Chem. Phys.* **1992**, *166*, 411–424.
- (70) Bodeur, S.; Hitchcock, A. Inner- and valence-shell excitation of SF₄ studied by photoabsorption and electron energy loss spectroscopy. *Chem. Phys.* **1987**, *111*, 467–479.
- (71) Bodeur, S.; Marechal, J. L.; Reynaud, C.; Bazin, D.; Nenner, I. Chlorine K shell photoabsorption spectra of gas phase HCl and Cl₂ molecules. *Z. Phys. D: At., Mol. Clusters* **1990**, *17*, 291–298.
- (72) Lindle, D. W.; Cowan, P. L.; Jach, T.; LaVilla, R. E.; Deslattes, R. D.; Perera, R. C. C. Polarized x-ray emission studies of methyl chloride and the chlorofluoromethanes. *Phys. Rev. A* **1991**, *43*, 2353–2366.
- (73) Zubavichus, Y.; Shaporenko, A.; Korolkov, V.; Grunze, M.; Zharnikov, M. X-ray absorption spectroscopy of the nucleotide bases at the carbon, nitrogen, and oxygen K-edges. *J. Phys. Chem. B* **2008**, *112*, 13711–13716.
- (74) Frati, F.; Hunault, M. O.; De Groot, F. M. Oxygen K-edge X-ray absorption spectra. *Chem. Rev.* **2020**, *120*, 4056–4110.
- (75) Plekan, O.; Feyer, V.; Richter, R.; Coreno, M.; De Simone, M.; Prince, K.; Trofimov, A.; Gromov, E.; Zaytseva, I.; Schirmer, J. A theoretical and experimental study of the near edge X-ray absorption fine structure (NEXAFS) and X-ray photoelectron spectra (XPS) of nucleobases: Thymine and adenine. *Chem. Phys.* **2008**, *347*, 360–375.
- (76) Tsuru, S.; Vidal, M. L.; Pápai, M.; Krylov, A. I.; Møller, K. B.; Coriani, S. An assessment of different electronic structure approaches for modeling time-resolved x-ray absorption spectroscopy. *Struct. Dyn.* **2021**, *8*, 024101.

- (77) Ehlert, C.; Gühr, M.; Saalfrank, P. An efficient first principles method for molecular pump-probe NEXAFS spectra: Application to thymine and azobenzene. *J. Chem. Phys.* **2018**, *149*, 144112.
- (78) Ehlert, C.; Klamroth, T. PSIXAS: a Psi4 plugin for efficient simulations of x-ray absorption spectra based on the transition-potential and Δ -Kohn–Sham method. *J. Comput. Chem.* **2020**, *41*, 1781–1789.